frontiers | Frontiers in Earth Science

TYPE Original Research
PUBLISHED 04 December 2024
DOI 10.3389/feart.2024.1494093

OPEN ACCESS

EDITED BY
Andrea Zanchi,
University of Milano-Bicocca, Italy

REVIEWED BY
Hu Li,
Sichuan University of Science and Engineering, China
Jaume Vergés,
Spanish National Research Council (CSIC), Spain

*CORRESPONDENCE
Wei Wang,
wangw@nigpas.ac.cn

RECEIVED 10 September 2024
ACCEPTED 18 November 2024
PUBLISHED 04 December 2024

CITATION
Chen W, Wang W, Zhao J, Yin H, Hu F, Zhang Y, Li Z, Jia D and Zhang C (2024) The geometry and evolution of the deeply buried structural wedge in the kuqa fold-and-thrust belt: insights from numerical simulation. *Front. Earth Sci.* 12:1494093. doi: 10.3389/feart.2024.1494093

The geometry and evolution of the deeply buried structural wedge in the kuqa fold-and-thrust belt: insights from numerical simulation

Weili Chen[1], Wei Wang[2]*, Jiaqi Zhao[1], Hongwei Yin[3], Fangjie Hu[1], Yong Zhang[2], Zhihao Li[1], Dong Jia[3] and Chunbo Zhang[1]

[1]Research Institute of Petroleum Exploration and Development, Tarim Oilfield Company, Korla, China, [2]State Key Laboratory of Palaeobiology and Stratigraphy, Nanjing Institute of Geology and Palaeontology, Chinese Academy of Sciences, Nanjing, China, [3]School of Earth Science and Engineering, Nanjing University, Nanjing, China

Numerical simulation is used to investigate the influence of thickness variation on the evolution of buried structural wedges, representing structures formed between two detachments. Simulations are based on the Kuqa fold-and-thrust belt, characterized by a tapered sedimentary sequence. Two sets of models were developed, one considering syn-tectonic sedimentation and the other without it. Model results indicate that an increase in thickness leads to larger intervals of thrusts, larger-scale thrust anticlines, and a reduced number of thrusts within the buried structural wedge, regardless of the presence of syn-tectonic sedimentation. The presence of syn-tectonic sedimentation is found to constrain the propagation of deformation within buried structural wedges, while increased thickness is observed to promote deformation propagation. Model results show that the deformation front expands toward the foreland from the thin model to the medium model and withdraws from the medium model to the thick model. This suggests that with the increase of wedge thickness, the restriction influence of syn-tectonic sedimentation on deformation propagation is more obvious than promotion. Model results show similarities in the structural features with the buried structural wedge in the Kuqa fold-and-thrust belt. With insights from numerical simulation, we suggest that the increased Mesozoic strata thickness from the west to east controls the structural variation along the strike. In the east, there are fewer thrust faults and larger fault intervals. Due to the restriction influence of the syn-tectonic sedimentation on the deformation propagation, the deformation front is an arc shape in the map view from west to east.

KEYWORDS

deformation propagation, thickness variation, numerical simulation, kuqa depression, structural wedges, fold-and-thrust belts

1 Introduction

Structural wedges, which consist of closely packed thrust sheets in fold-and-thrust belts and accretionary wedges, are a key focus of research due to their widespread occurrence worldwide. Examples include the Alpine-Himalayan system (Caméra et al., 2017; Cifelli et al., 2016; Qayyum et al., 2015; Yin, 2006), The South Pyrenean Central Salient (Ford et al., 2022; Lacombe et al., 2022; Muñoz et al., 2013; Sussman et al., 2004), The Zagros fold-and-thrust belt (Le Garzic et al., 2019; McQuarrie, 2004; Sherkati et al., 2006), and the Keping fold and thrust belt (Zhang et al., 2019). The geometry and dynamics of structural wedges play a crucial role in various geological processes such as hydrocarbon accumulation (Fan et al., 2020; Fan et al., 2024; Liu et al., 2019; Ryan et al., 2017), tectonic evolution (He et al., 2023b; Hubert-Ferrari et al., 2007; Zhou and Zhou, 2022), and earthquake assessment (Barchi et al., 2021; Lu et al., 2016). Studies have shown that the evolution of structural wedges is controlled by many factors [e.g., detachment rheology (Pla et al., 2019; Ruh et al., 2012), surface process (Konstantinovskaya and Malavieille, 2011; Wang et al., 2022), mechanical stratigraphy (Dean et al., 2013), and inherited structures (Wu et al., 2014; Yang et al., 2024)]. This paper mainly focuses on the thickness variation of the deformed strata, which is also a primary parameter controlling the structural evolution in natural structures (Jiao et al., 2021; Santolaria et al., 2022; Santolaria et al., 2024).

Using analog modeling and numerical simulations, the influence of thickness variation above the detachment has been tested in different model set-ups, including the sharp transition, gradual transition, and other complex models (Calassou et al., 1993; Jiao et al., 2021; Santolaria et al., 2022; Santolaria et al., 2024; Sun et al., 2016). Previous studies suggest that the increased thickness of the overburden units can affect the deformation propagation with larger structural intervals, less thrust faults, and longer deformation front (Marshak and Wilkerson, 1992; Soto et al., 2002).

However, previous studies mainly focus on the structural wedges with sedimentary covers deforming along a basal detachment, and the buried structural wedge developed in multiple detachments system has rarely been discussed. The buried structural wedges mainly develop in duplex structures. The deformation is separated by lower and upper detachments, and a structural wedge develops between them (Baby et al., 1992; Banks and Warburton, 1986; Couzens-Schultz et al., 2003; Mitra, 1986). The buried structural wedge deforms along the lower detachment. The buried structural wedge exhibits quite different features in geometry and kinematics from the systems with single detachment. More intense deformation is formed by imbricate thrust faults (Couzens-Schultz et al., 2003; Li et al., 2017).

In this study, numerical simulations are used to test the influence of strata thickness on the deformation of the buried structural wedges, using the Kuqa fold-and-thrust belt as an example. Two detachments control the deformation of the Kuqa fold-and-thrust belt, with a salt layer decoupling the deformation above and below it as the upper detachment. (Izquierdo-Llavall et al., 2018; Pla et al., 2019; Qi et al., 2023; Tang et al., 2004a; Wang et al., 2017; Wang et al., 2011). A long-propagated fold belt develops above the upper detachment, and a buried structural wedge consisting of imbricate thrusts forms above the lower detachment.

The buried structural wedge shows varied geometries with the strata thickness increases from west to east along the strike. Based on the seismic interpretation, the structural variation along the strike has been described. Then, a numerical simulation program was designed according to the stratigraphy of the Kuqa fold-and-thrust belts. The setup contains two detachments, and two model suites were carried out with and without syn-tectonic sedimentations. Each model suite includes three models, with different intermediate layer thicknesses between two detachments.

By comparing the model results with the structural features of the Kuqa depression, this study highlights the control of Mesozoic strata thickness on structural variations along the strike in the Kuqa fold-and-thrust belt. Besides, the simulations also provide insights into the structural evolution of fold-and-thrust belts containing two detachments. This is not only helpful to understanding the geometry and kinematics of multiple detachment systems, but also useful to the structural interpretation and hydrocarbon exploration in such structures.

2 Geological setting

The Kuqa fold-and-thrust, located in the northern Tarim basin, developed a Cenozoic multiple detachments system (Figure 1). The Cenozoic and Mesozoic successions are involved in the Cenozoic deformation, which mainly consists of clastic sediments, including conglomerate, sandstone, and mudstone (Neng et al., 2018; Pla et al., 2019; Qi et al., 2023) (Figure 2).

Previous studies suggest that the deformation of the Kuqa fold-and-thrust belt is controlled by two detachment systems (Chen et al., 2004; Gao et al., 2020; Li et al., 2021; Li et al., 2014; Tang et al., 2004b; Wang et al., 2011; Yu et al., 2008). The salt layer located at the lower part of Cenozoic stratigraphy acts as the upper detachment and the base of Mesozoic acts as the basal detachment (He et al., 2023a; Long et al., 2021; Wang et al., 2023; Wang et al., 2017; Yang et al., 2024). The salt layer decouples the deformation in the units above and below it. A board deformation zone consists of gentle detached folds developed in the suprasalt units with the salt layer as the upper detachment, and a tight deformation zone containing imbricate thrusts forms in the subsalt units. Two salt layers develop in this region, the Paleogene Kumugeliemu salt layer in the western zone and the Neogene Jidike salt layer in the eastern zone (Adeoti and Webb, 2022; Li et al., 2021; Li et al., 2012; Neng et al., 2018; Wang et al., 2011; Wu et al., 2014; Yang et al., 2024). The Kumugeliemu salt layer is thicker and broader than the Jidike salt layer (Pla et al., 2019; Wang et al., 2023).

The geological map shows two strong deformation belts in the suprasalt units, the Kelasu structural belt and the Qiulitage structural belt. However, the deformation in the subsalt units occurs in the Kelasu structural belt (Figure 1). The subsalt units show varied structural features along the strike with similar deformation backgrounds. From the western zone to the central zone, the deformation front moves toward the foreland and then withdraws slightly from the central zone to the eastern zone. The number of faults decreases from the west to east in general.

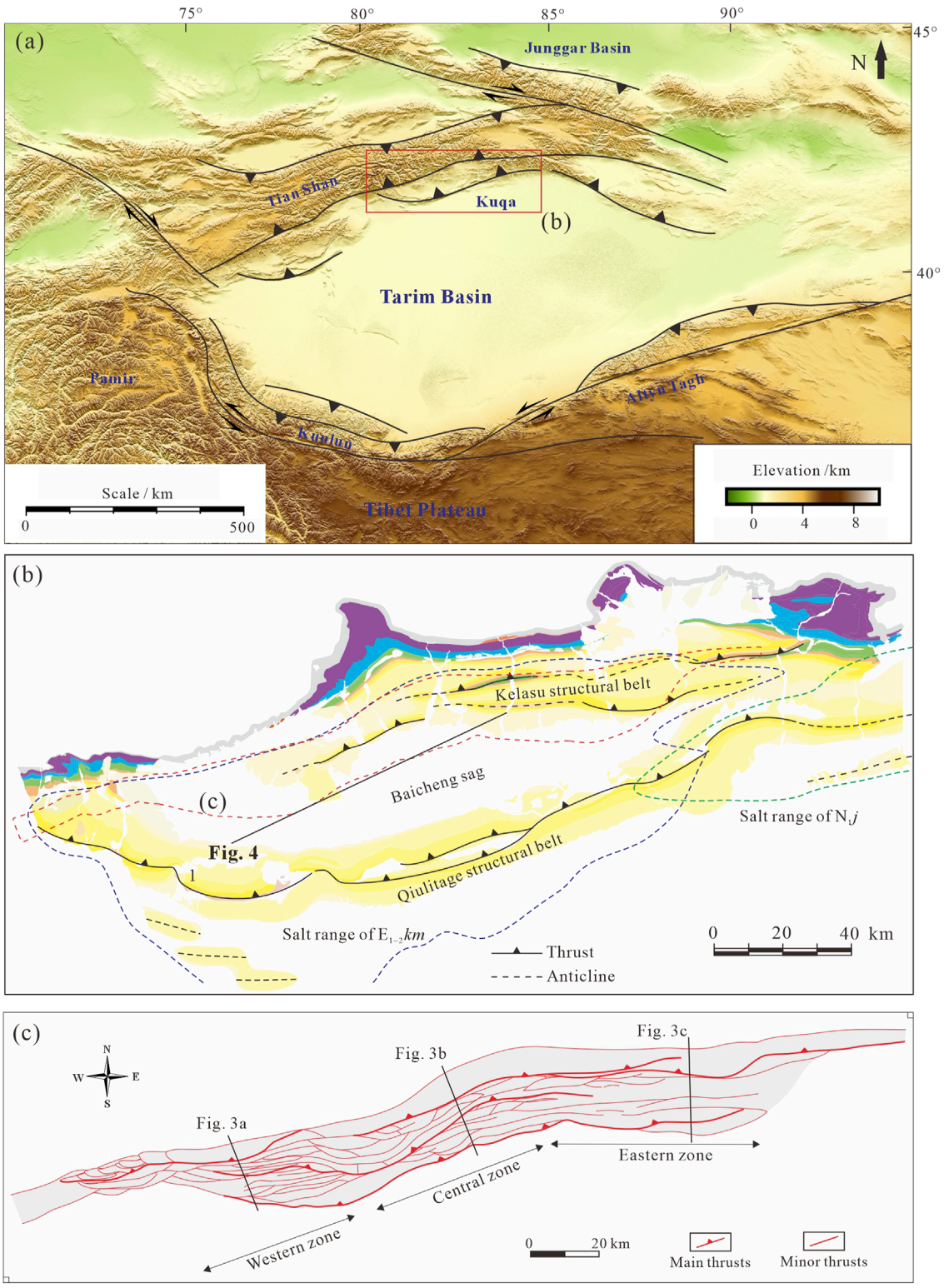

FIGURE 1
The geological map of the Kuqa fold-and-thrust belt and the subsalt system at the top Cretaceous. **(A)** Elevation map showing tectonic sketch of the central Asia and the location of the Kuqa fold-and-thrust belt. **(B)** Geological map of the Kuqa fold-and-thrust belt. **(C)** Subsalt fault system at the top Cretaceous in the Kelasu structural belts. The range is indicated in Figure 1B.

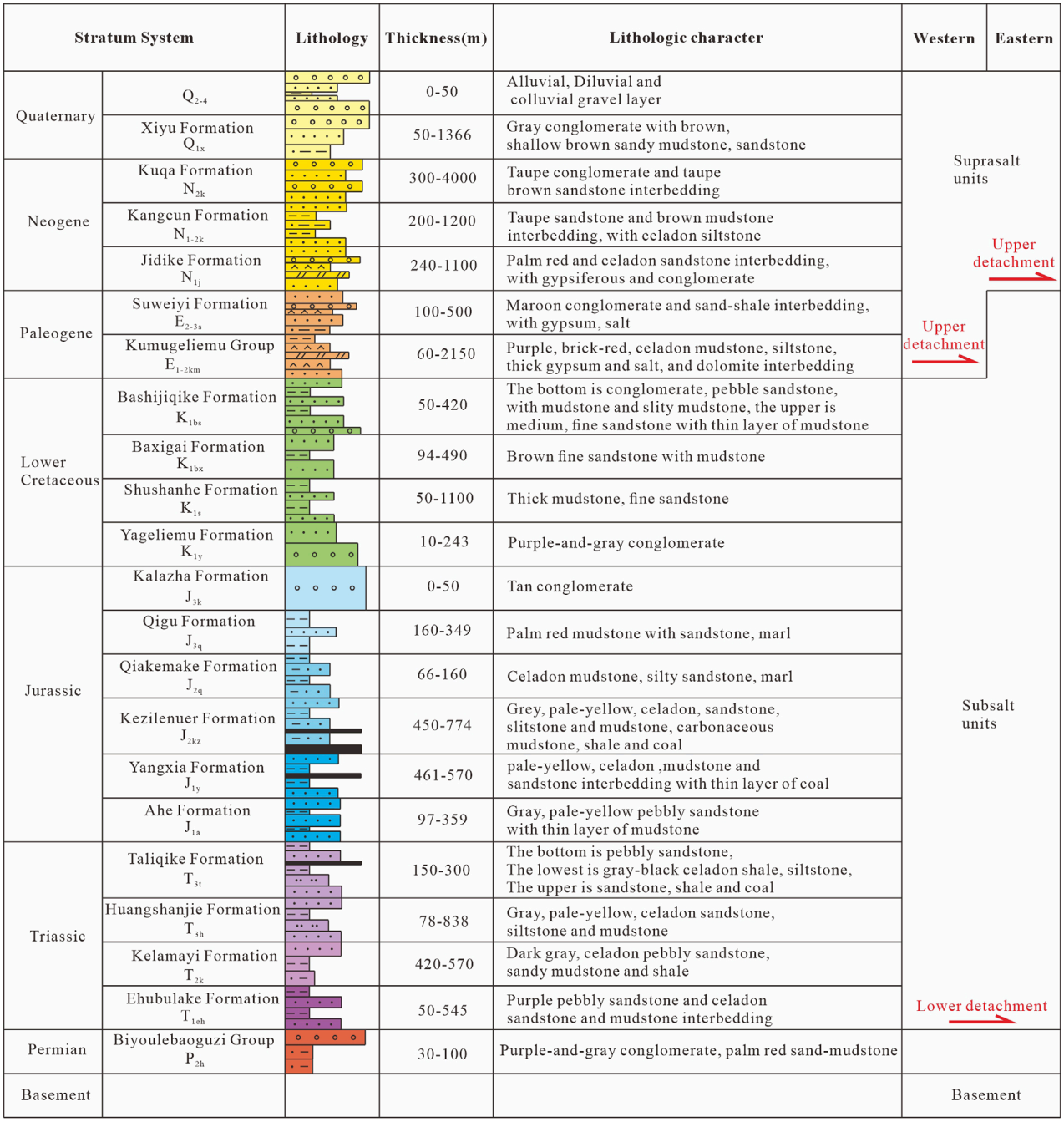

FIGURE 2
Strata column of the Kuqa depression (modified from Wang et al., 2017). Two salt layers are deposited in the Kuqa depression acting as the upper detachment. The Paleogene salt layer is in the western zone and the Neogene salt layer is in the eastern zone. The range is indicated in Figure 1.

3 Structural features

The Kelasu structural belt is located in the western of the Kuqa depression. Structural geometries and kinematics show apparent differences along the strike. Three seismic profiles are interpreted to show the structural features (Figure 3). The seismic-well correlation is used to determine the tops of strata, which is introduced in Wang et al. (2023). The interpreted structural model of the Kelasu structural belt is mainly controlled by two detachments, which is consistent with previous studies (He et al., 2023a; Wang et al., 2023; Wang et al., 2017; Wang et al., 2020). The thick Kumugeliemu salt layer acts as the upper detachment, and the shales at the bottom of Mesozoic strata as the basal detachment. Considering the salt layer could form salt structures during the deformation, the structural units are divided into four parts: suprasalt units, salt layer, subsalt structural wedge, and basement units.

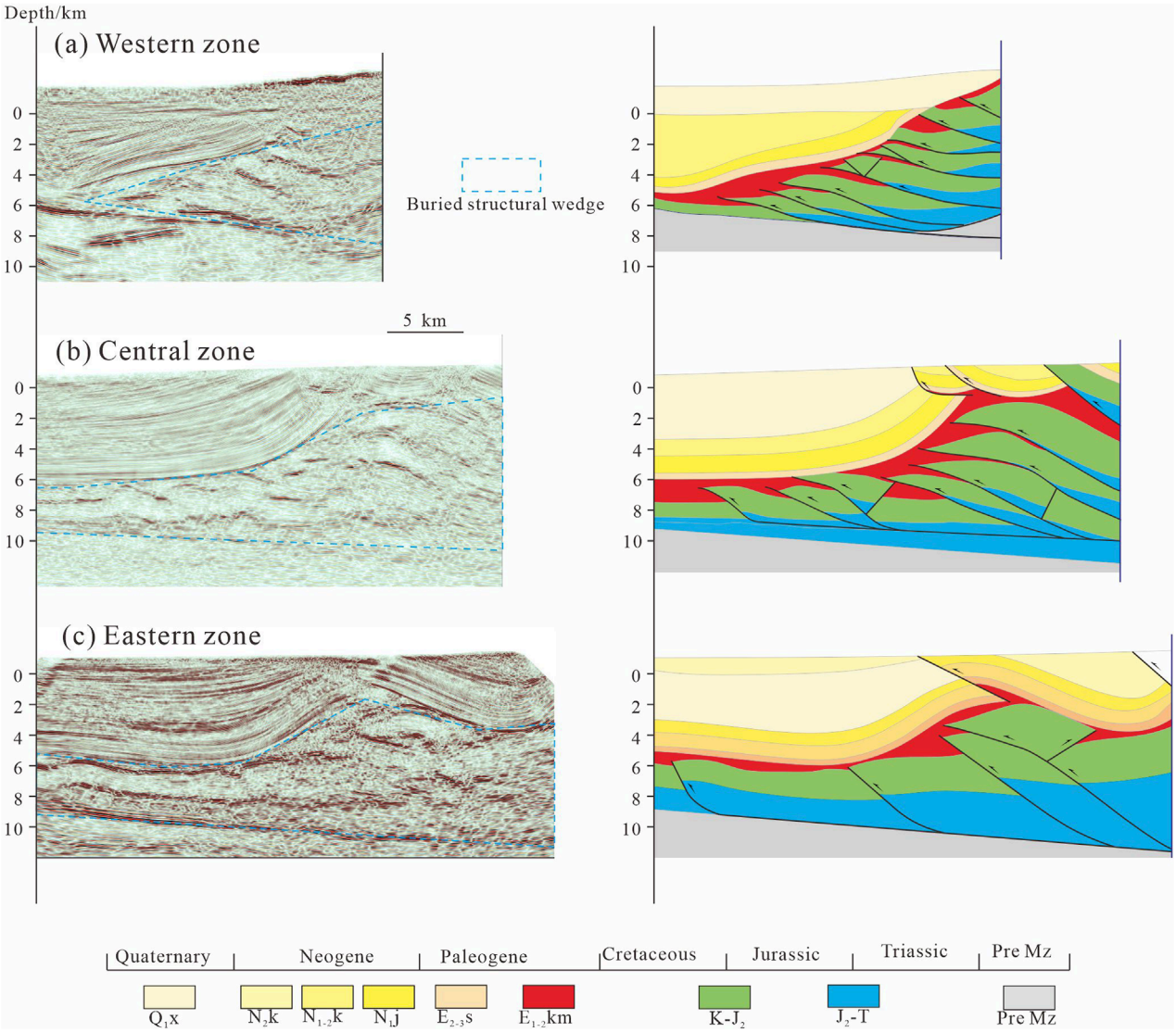

FIGURE 3
Cross-sections showing the structural variation in the western **(A)**, central **(B)**, and eastern **(C)** zones of the Kelasu structural belt.

The difference in the suprasalt unit is mainly expressed as the number of structures and sedimentation records. The geological map of the Kuqa depression shows a varied number of folds along the trike in the Kelasu structural belt (Figure 1A). No fold develops in the western zone, while one thrust-related fold occurs toward the central zone. Two folds form in the eastern zone, but the distance between the two folds increases from the west to the east. In the cross-sections, suprasalt units also show different features (Figure 3). The sedimentation of the western zone shows a changed depocenter from the north to south, and then the Quaternary units cover the previous units uniformly. The central and eastern zones both develop a detached fold with the salt layer as the detachment. The long interval between the two folds forms a board syncline between them in the eastern zone.

The salt layer shows similar features in all three cross sections. The salt layer acts as the upper detachment layer decoupling the deformation above and below it. Some salts accumulate in the core of the anticline and salt welding develops above the anticlines of subsalt units. The subsalt units mainly consist of thrust sheets and the main difference is the number and scale of thrust sheets. Generally, the interval and scale increase from the west to the east. Specifically, the interval of thrusts is about 2 km in the western zone, 3–4 km in the central zone, and over 6 km in the eastern zone.

According to the seismic profiles, the thickness of the subsalt Mesozoic units increases from the basin to the orogenic. The eastern zone develops the least thrusts in the subsalt units. The clear reflection shows that the thickness of the subsalt unit increases from 4 km to 5 km, with the location moving 10 km toward the orogenic belt (Figure 3C). Besides, the thickness of the subsalt units also increases along the strike. The seismic profile along the strike shows that the thickness of subsalt Mesozoic units increases from about

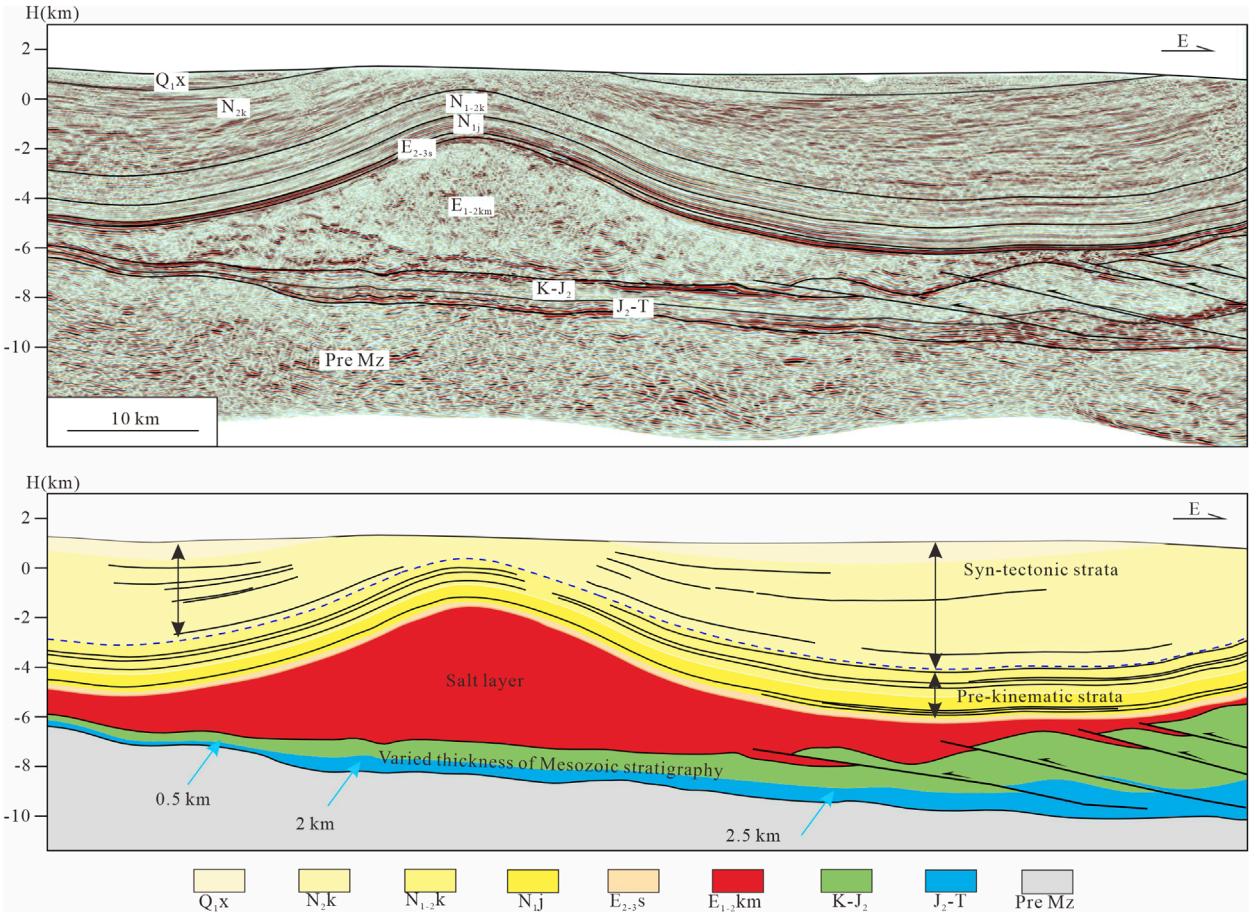

FIGURE 4
Seismic profile along the strike showing the construction of pre-kinematic strata, syn-tectonic strata, and the varied thickness of Mesozoic stratigraphy below the salt layer.

0.5 km in the western zone to 2 km in the central zone, and then to 2.5 km in the eastern zone (Figure 4).

4 Methodology

The discrete element method (DEM) is a particle-based numerical method that simplifies natural structure into an assemblage of balls. The balls move to follow Newton's equations under the compression or extension of boundaries. The DEM method has been detailly introduced by Morgan (2015) and has been widely used to investigate the deformation of fold-and-thrust belts in previous studies (Morgan, 2015; Wang et al., 2022; Zhang et al., 2013). The Version of DEM used in this study is ZDEM (Li et al., 2021), which is developed according to the RICEBAL (Morgan, 2015) and the open-source code TRUBAL (Cundall and Strack, 1979).

The models consisted of balls with radii of 60 m and 80 m. The bulk mechanical properties of the numerical material are determined according to the interaction of particles. The models in this paper contain two types of materials, the clastic sediments and the salt layer. The clastic sediments are represented by the bonded balls, and the particle properties of the balls are based on the natural data and previous studies (Table 1) (Morgan and Bangs, 2017). The salt layer is mechanically weak and flows like a fluid (Hudec and Jackson, 2007). The unbonded particles are used to represent it, as previous studies demonstrate similar ductile behaviors during deformation when the friction coefficient is zero (Dean et al., 2015; Maxwell, 2009).

Common particle properties: shear modulus 2.9E09 Pa, Poisson's ratio 0.2, Time step 0.05 s, Wall velocity 1 m/s, Local damping coefficient 0.4, Gravitational acceleration 9.8 m/s ^{2}.

5 Numerical simulation

5.1 Model setup

This paper's main focus is on the influence of subsalt layer thickness on the deformation of salt-bearing fold-and-thrust belts. The model setup is based on the Kuqa fold-and-thrust

TABLE 1 Particle properties and interparticle bond properties in the DEM simulation.

	Friction coefficient	Density (kg/m^3)	Viscosity (pa·s)	Young's modulus (Pa)	Shear modulus (Pa)	Tensile strength (Pa)	Cohension (Pa)
Clastic sediments	0.3	2,500	—	2.0E08	2.0E08	4.0E07	8.0E07
Upper detachment (salt)	0.0	2,200	$10^{8-10(c)}$	—	—	—	—
Basal detachment	0.2	—	—	—	—	—	—

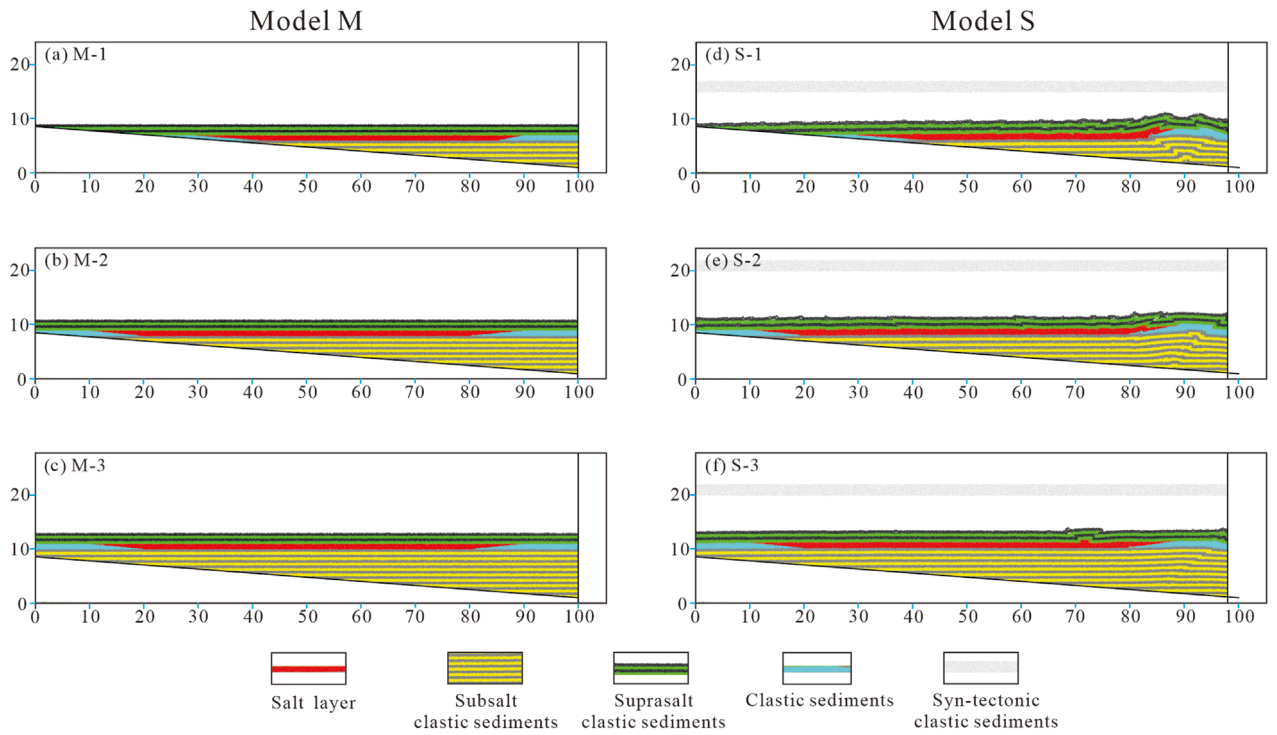

FIGURE 5
Model setup of numerical simulations. Model M contains three models without syn-tectonic sedimentations, and model S contains three models with syn-tectonic sedimentations.

belt and contains two detachments. A 1 km thickness consisting of unbonded balls is used to simulate the salt layer, and the bottom boundary with a friction coefficient of 0.2 represents the basal detachment. The initial model length is 100 km, and the thickness of suprasalt units is 2 km. Three models are derived with the same model setup except for the thickness of the subsalt units. The subsalt thickness is 5, 7, and 9 km, respectively (Figure 5).

Two model suites have been derived in this paper. The model suite M does not consider the influence of the syn-tectonic sedimentation, and the model suite S contains the syn-tectonic sedimentations (Table 2). The syn-tectonic sedimentations were added after each 2 km of shortening. The total shortening is 30 km, and 15 layers were deposited as growth strata. The balls in syn-tectonic layers had the same properties as clastic sediments (Table 1).

TABLE 2 Variation of the subsalt units and syn-tectonic sedimentation in different models.

	M-1	M-2	M-3	S-1	S-2	S-3
Suprasalt units/km	2	2	2	2	2	2
Subsalt units/km	5	7	9	5	7	9
Syn-tectonic sedimentation	No	No	No	Yes	Yes	Yes

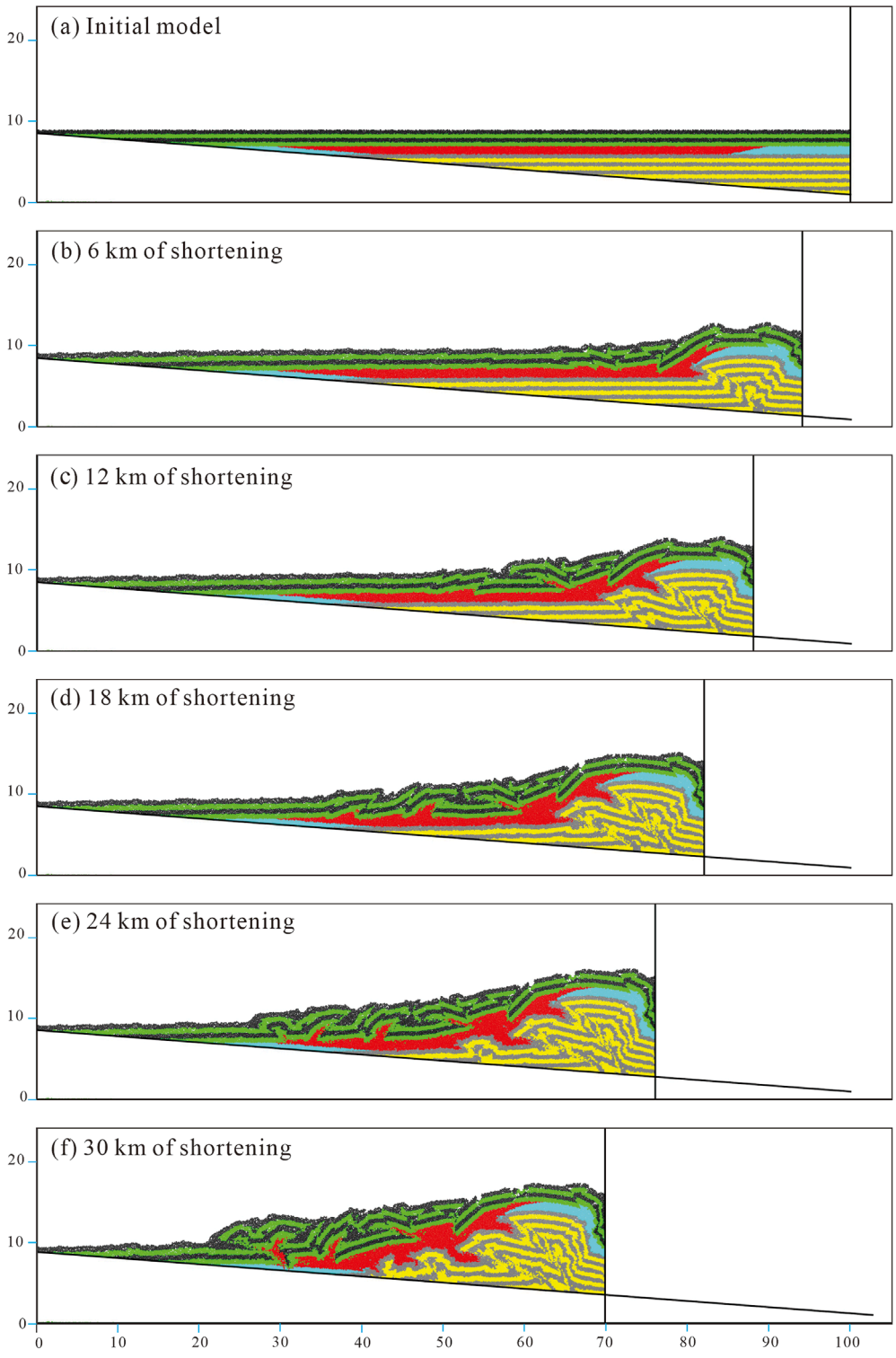

FIGURE 6
The evolution process of Model M-1. The **(A–F)** represents the geometry at the shortening of 0, 6, 12, 18, 24, and 30 km, respectively.

Each syn-tectonic layer had a thickness of 2 km generation and was approximately 1 km after sedimentation under gravity. A remove line was settled for each stage and the balls above the line were removed to simulate the natural growth strata that have an increased thickness from low to high. The removed line had a constant angle of 3.67° and a 0.4-km height increase at the next stage. Then, balls of syn-tectonic sedimentary layers were also bonded as clastic sediments (Table 1).

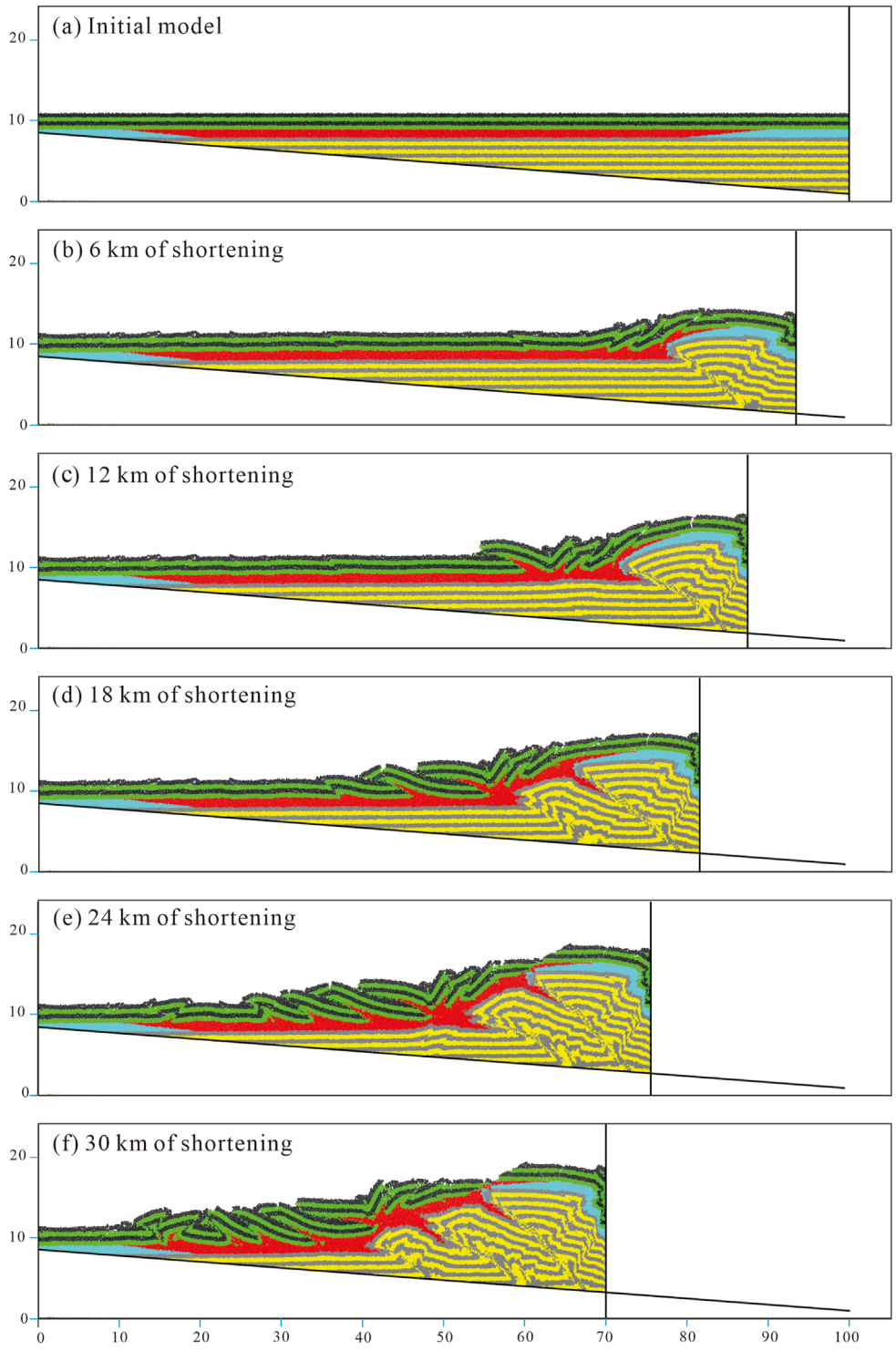

FIGURE 7
The evolution process of Model M-2. The **(A–F)** represents the geometry at the shortening of 0, 6, 12, 18, 24, and 30 km, respectively.

5.2 Model results

In model suite M, the evolution in all three models shows some similar features (Figures 6–8). The tight thrusts develop in the suprasalt units and the subsalt units. The deformation propagation is longer in the suprasalt units compared with the subsalt units. Different structural features also appear in suprasalt and subsalt units. Suprasalt units in Model M-1 mainly develop pop-up structures, while Model M-2 and M-3 mainly develop imbricated thrusts. Subsalt units show differences in the scale and number of thrusts.

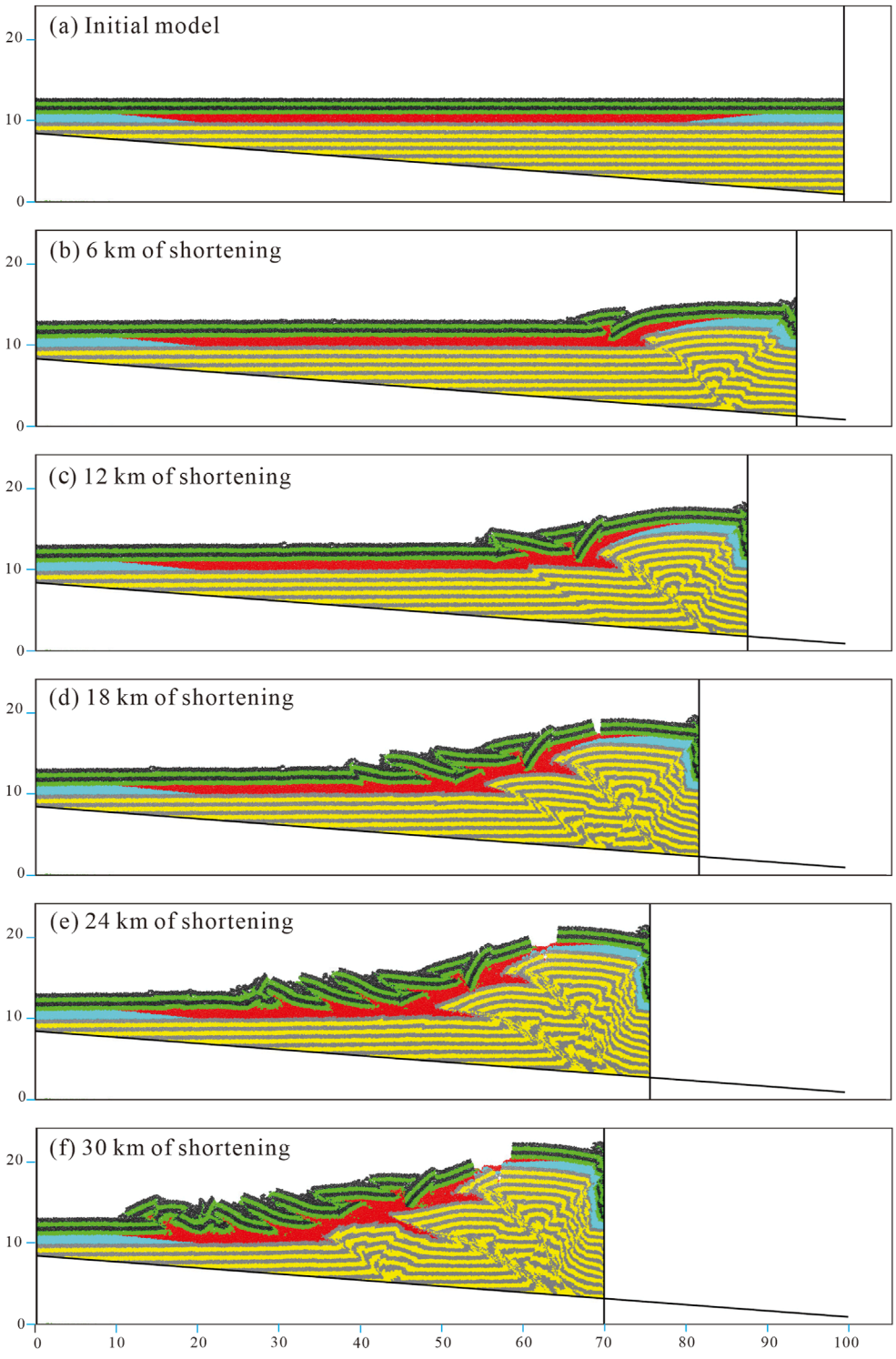

FIGURE 8
The evolution process of Model M-3. The **(A–F)** represents the geometry at the shortening of 0, 6, 12, 18, 24, and 30 km, respectively.

In model suite S (Figures 9–11), the suprasalt units show quite different features from the model suite M. Two main folds form in the suprasalt units, and the depocenter migrates toward the moving wall from model S-1 to S-3, with the thickness of subsalt units increasing. This reveals the deformation propagation speed toward the foreland. The difference in subsalt units also appears in the scale and number of thrusts. To better analyze the model results, quantitative investigations were carried out in the subsequent discussion.

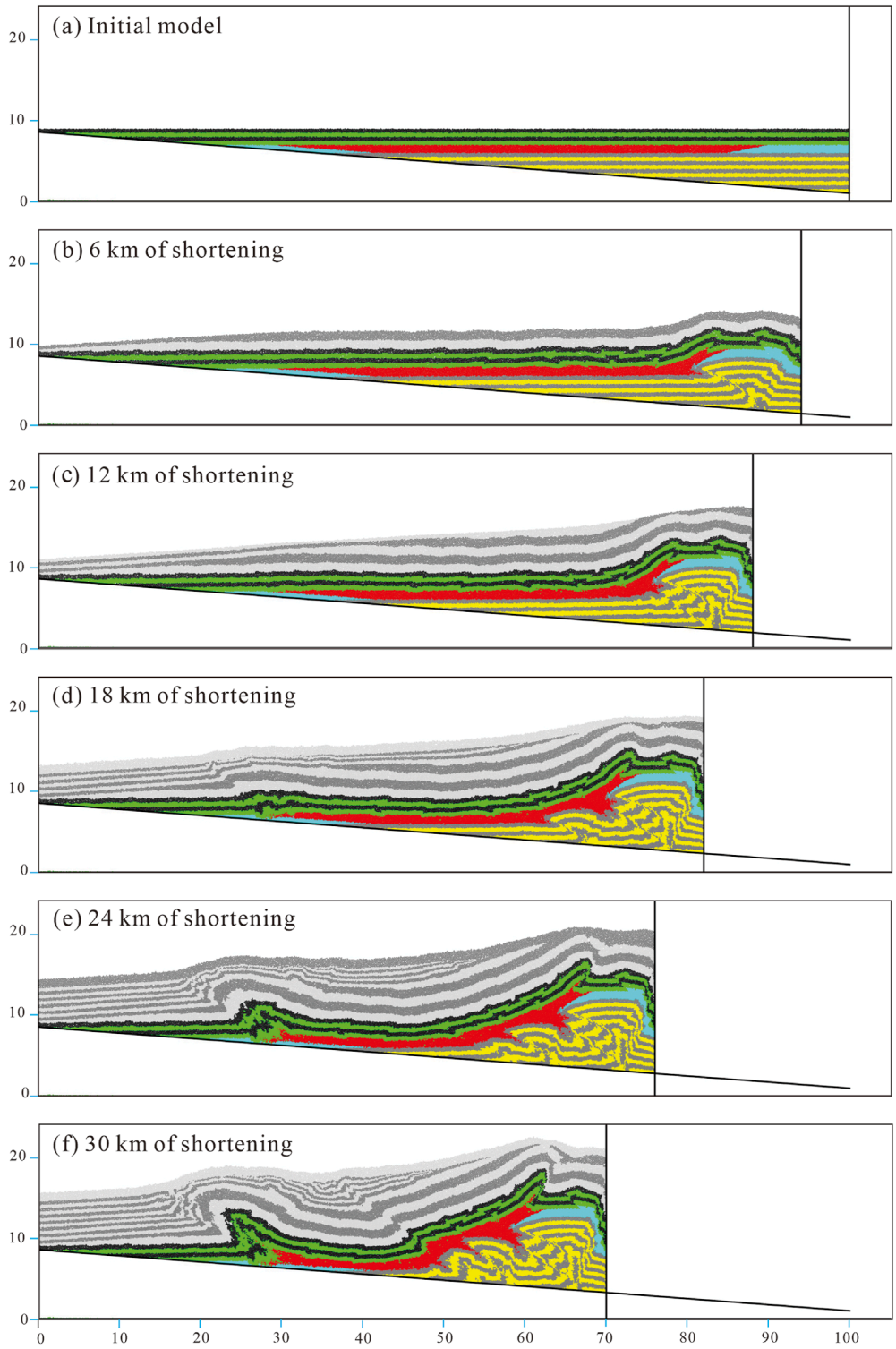

FIGURE 9
The evolution process of Model S-1. The **(A–F)** represents the geometry at the shortening of 0, 6, 12, 18, 24, and 30 km, respectively.

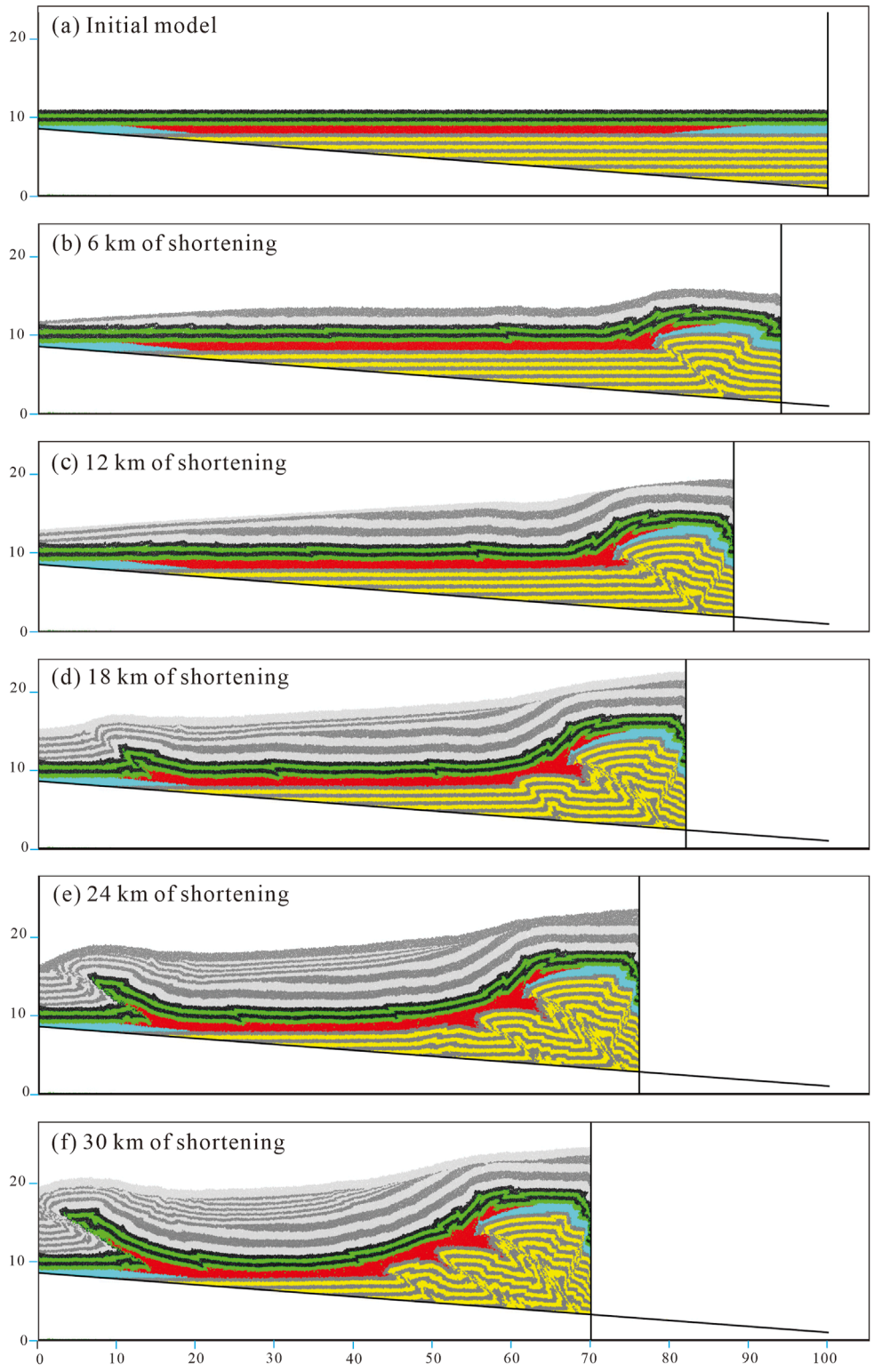

FIGURE 10
The evolution process of Model S-2. The **(A–F)** represents the geometry at the shortening of 0, 6, 12, 18, 24, and 30 km, respectively.

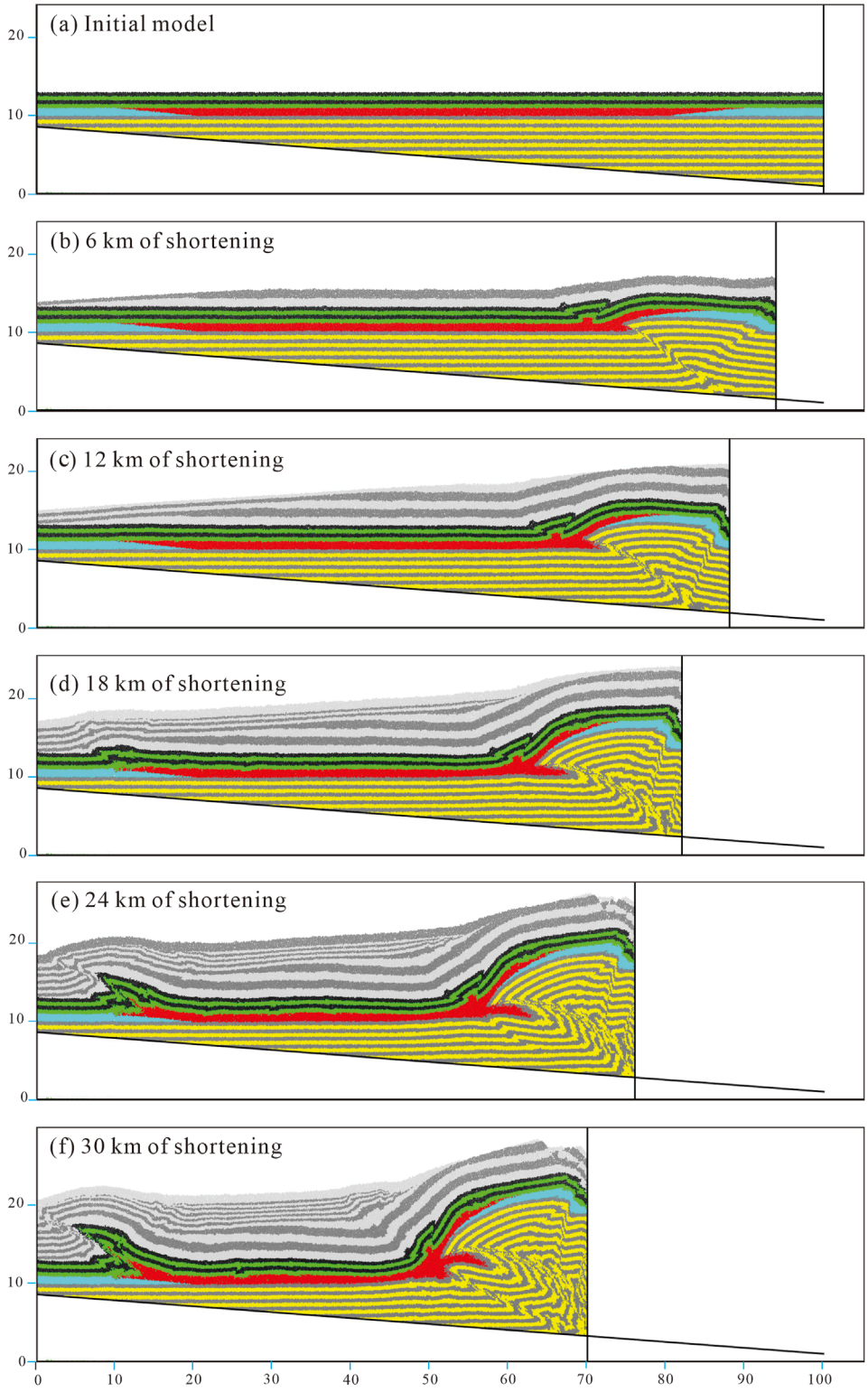

FIGURE 11
The evolution process of Model S-3. The **(A–F)** represents the geometry at the shortening of 0, 6, 12, 18, 24, and 30 km, respectively.

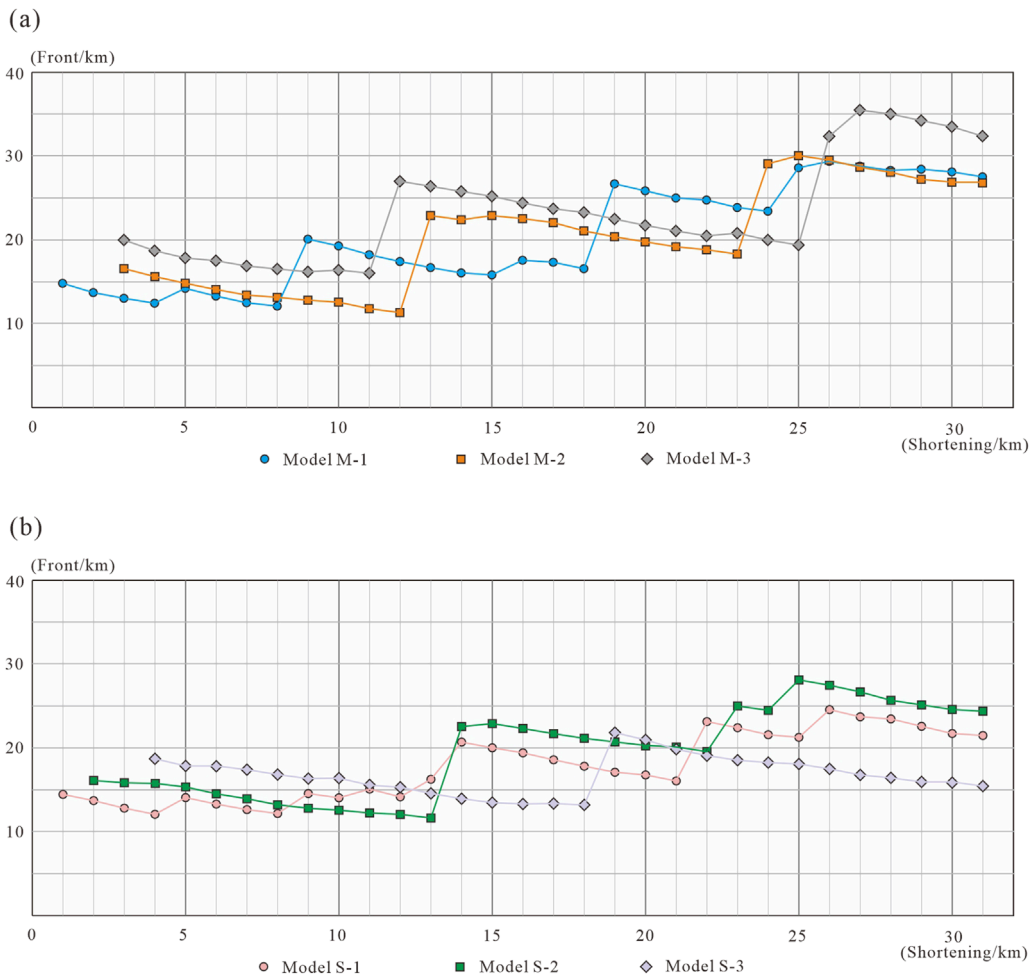

FIGURE 12
Deformation front propagation as the shortening increases of the models. **(A)** Model series without syn-tectonic sedimentation. **(B)** Model series with syn-tectonic sedimentation.

6 Discussion

6.1 Influence of thickness on the deformation of the subsalt structural wedge without syn-tectonic sedimentation

Previous studies suggest that the deformation front propagation in structural wedge is episodic (Bigi et al., 2010). Analog modeling further proposes alternant front propagation in a model with changed layer thickness (Zhang et al., 2019). The numerical simulation shows that buried structural wedges also have similar features in the deformation front propagation (Figure 12A). The deformation front in M-1 is farther than M-2 when the shortening is from 9 km to 12 km. An obvious difference also exists between the previous analog modeling (Zhang et al., 2019) and the numerical simulation in this paper. The deformation front always changes when a new fault forms in the numerical simulation, which barely happens in the analog modeling. Numerous reasons may lead to this divergence, the different methods, tapered stratigraphy, and buried structural wedges.

The increased initial thickness of the subsalt wedge causes the increased scale of thrust sheets. This can be identified in the different parts within one model or in different models with varied thicknesses (Figure 13). For example, four fault-related folds develop in the subsalt units of model M-1, the fold above F2 near the hinterland is about 6 km wide while the fold above F4 near the foreland is about 2 km wide. As for the different models, the width of the fold above F3 is about 2 km, 4 km, and 10 km in M-1, M-2, and M-3, respectively.

The increased initial thickness of the subsalt wedge causes the increased intervals of thrust sheets. The distance between the F2 and F3 is about 4 km in model M-1, 10 km in model M-2, and 14 km in model M-3. Besides, the increased thickness also forms fewer faults or fault-related folds, four thrust-related folds formed in M-1, but only three thrust-related folds formed in M-2 and M-3.

Furthermore, the distortional strain distribution shows that the thick layer thickness tends to form an intact fold, while the fold formed in a thin layer region contains more secondary faults (Figure 13). For example, the fold along F3 contains three backthrusts and two secondary thrusts in model M-3, while no secondary fault develops in the fold along F2. Compared with M-3, the M-1 and M-2 also develop more secondary faults in the thrust-related folds.

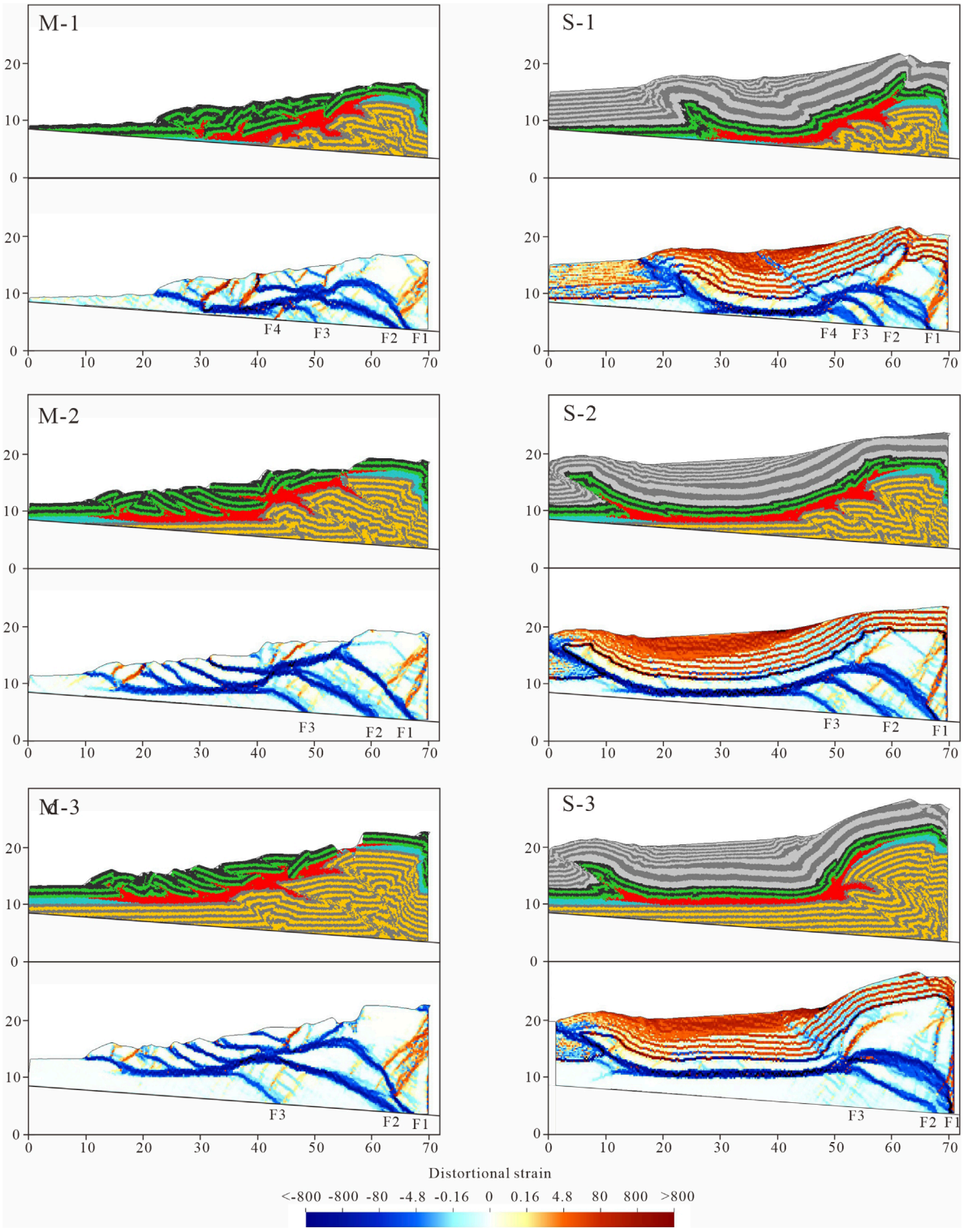

FIGURE 13
Structural geometry and distortional strain of six models at the shortening of 30 km. The red indicates the top-to-right sense of shear, and the blue indicates the top-to-left sense of shear.

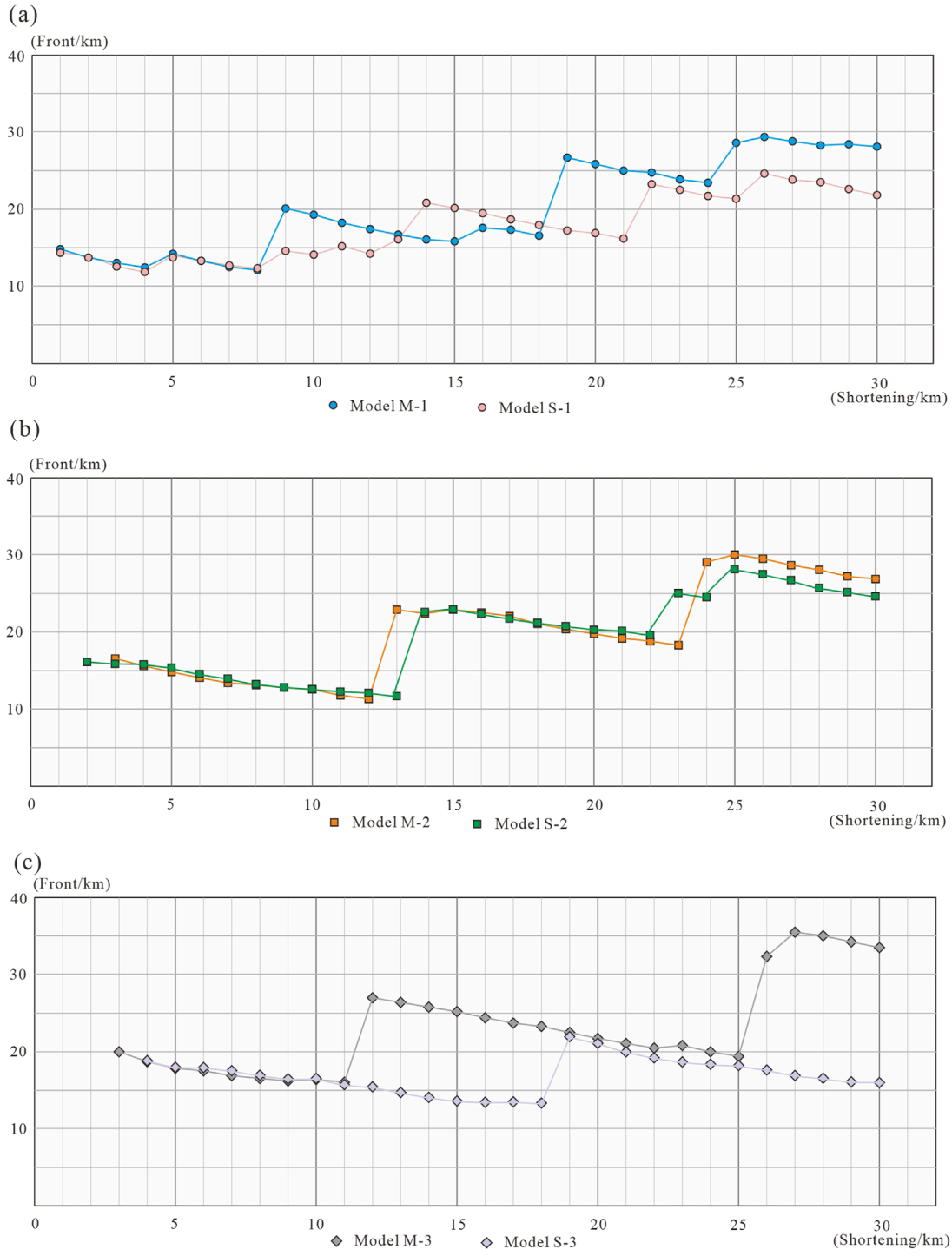

FIGURE 14
Comparison between the deformation front propagation between **(A)** model M-1 and S-1, **(B)** model M-2 and S-2, and **(C)** model M-3 and S-3. This reveals the varied influence of syn-tectonic sedimentation on the deformation propagation when the initial thickness of buried structural wedges changes.

6.2 Influence of syn-tectonic sedimentation on the evolution of subsalt structural wedge

The comparison between the deformation propagation process of models with and without the syn-tectonic sedimentations shows that the syn-tectonic sedimentation can restrict the deformation propagation (Figure 12). The deformation front is closer to the moving wall in all three models with syn-tectonic sedimentation. Our model results further show that the strength of restriction seems to vary with the increase of the total shortening and initial thickness. As for the total shortening, the restriction influence

of syn-tectonic sedimentation on the deformation propagation appears at the shortening of 9 km in model S-1, 13 km in model S-2, and 12 km in model S-3 (Figure 14). The reduced amount of deformation front keeps increasing in general. The restriction influence of syn-tectonic sedimentation on the deformation front is much stronger in the model with a thick initial thickness. The reduced amount of deformation front is about 5 km in model 1, and 2 km in model 2, and increases sharply to about 18 km in model 3 (Figure 14).

The comparison between the deformation propagation process of models with and without the syn-tectonic sedimentations shows the divergence. Model S-2 shows an increased deformation front compared with S-1, while the S-3 shows a decreased deformation front compared with the S-2 and S-1 since the shortening reached 14 km (Figure 12). This phenomenon reveals the overlaid influence of increased initial thickness and syn-tectonic sedimentation on the deformation propagation. The increased thickness can promote deformation propagation, while the syn-tectonic sedimentation restricts it for buried structural wedges. From Model S-1 to S-2, the deformation front increases representing the promotion of the increased thickness is larger than the restriction of syn-tectonic sedimentation. The deformation front withdraws from Model S-2 to S-3 largely, which suggests that the restriction influence increases faster than promotion when the initial thickness increases.

6.3 Implications for the structural variation of the kelasu structural belt

By comparing the model results with the Kelasu structure, the thickness variation of the Mesozoic units has a significant influence on the variation of the fault systems in the buried subsalt structural wedge. Narrow imbricated thrust sheets develop in the western zone of the Kelasu structural belt. The intervals between thrust sheets keep increasing, toward the central zone and eastern zone of the Kelasu structural belt. The influence of the thickness on the deformation not only exists along the strike but also along the direction of deformation propagation. The thrusts near the orogenic belts typically have larger intervals and scales.

A remarkable phenomenon is that the thick syn-tectonic sedimentation can impress the deformation propagation in the subsalt structural wedge. Critical wedge theory and previous analog modeling containing one basal detachment suggest that the increased layer thickness can produce a further deformation front. In our models, the subsalt structural deformation is restricted in the region near the hinterland in the M-3 which has the largest thickness, but propagates farther to the foreland in M-1 which has the least thickness (Figure 13). The Kuqa fold-and-thrust shows similar features as revealed by our models (Figure 3). The deformation propagation range increases sharply from the western zone to the central zone and then decreases slightly to the eastern zone. However, the faults near the foreland in the eastern zone have minor displacement compared with the western and central regions. Based on the numerical simulation results, we suggest that the thick syn-tectonic sedimentation restricts the subsalt deformation propagation in the eastern region.

6.4 Limitations

The evolution of the Kuqa depression is affected by many factors including the pre-existing salt diapir, paleo-uplift, and basement faults. This paper only focuses on the influence of the initial thickness of the subsalt wedge. Other factors have not been considered in the models, which could cause the difference between the model results and natural geometries. In addition, although the syn-tectonic sedimentation is included in models, the process is simplified. The erosion does not occur in our models. Besides, the influence of the uplift rate on the sedimentation rate has not been considered in the models. The model suite S has the same process of syn-tectonic sedimentation.

7 Conclusion

Based on the seismic interpretation and numerical simulation, we conclude as follows:

(1) The influence of thickness on the buried structural wedge shows similar features with and without syn-tectonic sedimentation. The increased thickness leads to enlarged intervals of thrusts, larger thrust anticlines, and fewer thrusts in both cases.

(2) The deformation front exhibits an inconsistent trend when the thickness variation is accompanied by syn-tectonic sedimentation. The increased thickness can promote deformation propagation, while the syn-tectonic sedimentation restricts the propagation of buried structural wedges. Our model results suggest that the dominant factor varies with the thickness increasing. The deformation front increased from the thin model to the medium model, which represents the advantage of propagation. The deformation front decreased from the medium model to the thick model, which represents the changed domination from propagation to restriction.

(3) Comparing the model results with the structural features of the Kelasu structural belt, we suggest that the increasing initial thickness of the buried wedge controls the structural variation from west to east. Fewer thrust faults form in the eastern zone with larger intervals. Due to the restriction influence of the syn-tectonic sedimentation on the deformation propagation, the deformation front of the buried structural wedge in the Kelasu structural belt is an arc shape in the map view from west to east.

Data availability statement

The original contributions presented in the study are included in the article/supplementary material, further inquiries can be directed to the corresponding author.

Author contributions

WC: Writing–original draft, Data curation, Resources. WW: Writing–review and editing, Conceptualization, Methodology, Software, Writing–original draft. JZ: Data curation, Formal Analysis, Investigation, Writing–original draft. HY: Conceptualization, Funding acquisition, Project administration, Software, Writing–review and editing. FH: Data curation, Investigation, Writing–original draft. YZ: Investigation, Methodology, Writing–review and editing. ZL: Data curation, Investigation, Writing–original draft. DJ: Writing–review and editing. CZ: Data curation, Investigation, Writing–original draft.

Funding

The author(s) declare that financial support was received for the research, authorship, and/or publication of this article. This work was supported by the National Natural Science Foundation of China (41972219, 41572187, 42102270, and 41927802), and the Fundamental Research Funds for NIGPAS (NGBS202422).

Acknowledgments

We appreciate editor Andrea Zanchi, and two reviewers Hu Li and Jaume Vergés for their instructive comments.

Conflict of interest

Authors WC, JZ, FH, ZL, and CZ were employed by Tarim Oilfield Company.

The remaining authors declare that the research was conducted in the absence of any commercial or financial relationships that could be construed as a potential conflict of interest.

Publisher's note

References

Adeoti, B., and Webb, A. A. G. (2022). Geomorphology of contractional salt tectonics along the Kuqa fold-thrust belt, northwestern China: testing pre-kinematic diapir versus source-fed thrust and detachment fold models. *J. Struct. Geol.* 161, 104638. doi:10.1016/j.jsg.2022.104638

Baby, P., Hérail, G., Salinas, R., and Sempere, T. (1992). Geometry and kinematic evolution of passive roof duplexes deduced from cross section balancing: example from the foreland thrust system of the southern Bolivian Subandean Zone. *Tectonics* 11 (3), 523–536. doi:10.1029/91tc03090

Banks, C., and Warburton, J. (1986). Passive-roof'duplex geometry in the frontal structures of the Kirthar and Sulaiman mountain belts, Pakistan. *J. Struct. Geol.* 8 (3-4), 229–237. doi:10.1016/0191-8141(86)90045-3

Barchi, M. R., Carboni, F., Michele, M., Ercoli, M., Giorgetti, C., Porreca, M., et al. (2021). The influence of subsurface geology on the distribution of earthquakes during the 2016–2017 Central Italy seismic sequence. *Tectonophysics* 807, 228797. doi:10.1016/j.tecto.2021.228797

Bigi, S., Di Paolo, L., Vadacca, L., and Gambardella, G. (2010). Load and unload as interference factors on cyclical behavior and kinematics of Coulomb wedges: insights from sandbox experiments. *J. Struct. Geol.* 32 (1), 28–44. doi:10.1016/j.jsg.2009.06.018

Calassou, S., Larroque, C., and Malavieille, J. (1993). Transfer zones of deformation in thrust wedges: an experimental study. *Tectonophysics* 221 (3-4), 325–344. doi:10.1016/0040-1951(93)90165-g

Caméra, J., Flinch, J., and Tari, G. (2017). *Permo-triassic salt provinces of europe, north africa and the atlantic margins: Part Iv alp folded belts*, 371. Tectonics and Hydrocarbon Potential.

Chen, S. p., Tang, L. j., Jin, Z. j., Jia, C. z., and Pi, X. j. (2004). Thrust and fold tectonics and the role of evaporites in deformation in the western Kuqa foreland of Tarim basin, northwest China. *Mar. Petroleum Geol.* 21 (8), 1027–1042. doi:10.1016/j.marpetgeo.2004.01.008

Cifelli, F., Caricchi, C., and Mattei, M. (2016). Formation of arc-shaped orogenic belts in the Western and Central Mediterranean: a palaeomagnetic review. *Geol. Soc. Lond. Spec. Publ.* 425 (1), 37–63. doi:10.1144/sp425.12

Couzens-Schultz, B. A., Vendeville, B. C., and Wiltschko, D. V. (2003). Duplex style and triangle zone formation: insights from physical modeling. *J. Struct. Geol.* 25 (10), 1623–1644. doi:10.1016/s0191-8141(03)00004-x

Cundall, P. A., and Strack, O. D. (1979). A discrete numerical model for granular assemblies: geotechnique. *Géotechnique* 29 (1), 47–65. doi:10.1680/geot.1979.29.1.47

Dean, S., Morgan, J., and Brandenburg, J. P. (2015). Influence of mobile shale on thrust faults: insights from discrete element simulations. *AAPG Bull.* 99 (03), 403–432. doi:10.1306/10081414003

Dean, S. L., Morgan, J. K., and Fournier, T. (2013). Geometries of frontal fold and thrust belts: insights from discrete element simulations. *J. Struct. Geol.* 53, 43–53. doi:10.1016/j.jsg.2013.05.008

Fan, C., Li, H., Qin, Q., He, S., and Zhong, C. (2020). Geological conditions and exploration potential of shale gas reservoir in Wufeng and Longmaxi Formation of southeastern Sichuan Basin, China. *J. Petroleum Sci. Eng.* 191, 107138. doi:10.1016/j.petrol.2020.107138

Fan, C., Nie, S., Li, H., Radwan, A. E., Pan, Q., Shi, X., et al. (2024). Quantitative prediction and spatial analysis of structural fractures in deep shale gas reservoirs within complex structural zones: a case study of the Longmaxi Formation in the Luzhou area, southern Sichuan Basin, China. *J. Asian Earth Sci.* 263, 106025. doi:10.1016/j.jseaes.2024.106025

Ford, M., Masini, E., Vergés, J., Pik, R., Ternois, S., Léger, J., et al. (2022). Evolution of a low convergence collisional orogen: a review of Pyrenean orogenesis. *Bull. Société Géologique Fr.* 193 (1), 19. doi:10.1051/bsgf/2022018

Gao, L., Rao, G., Tang, P., Qiu, J., Peng, Z., Pei, Y., et al. (2020). Structural development at the leading edge of the salt-bearing Kuqa fold-and-thrust belt, southern Tian Shan, NW China. *J. Struct. Geol.* 140, 104184. doi:10.1016/j.jsg.2020.104184

He, W., Wang, W., Xie, H., Yin, H., Jia, D., Xu, Z., et al. (2023a). The effects of salt flow on the cross-section restoration of salt-bearing fold-and-thrust belts: an example from the Kuqa depression. *J. Struct. Geol.* 167, 104795. doi:10.1016/j.jsg.2023.104795

He, W., Yu, Y., Luo, Y., and Li, S. (2023b). Effects of friction properties and rheological structures on the deformation patterns and evolution of fold-and-thrust belts—new insights from analogue modelling. *J. Struct. Geol.* 173, 104904. doi:10.1016/j.jsg.2023.104904

Hubert-Ferrari, A., Suppe, J., Gonzalez-Mieres, R., and Wang, X. (2007). Mechanisms of active folding of the landscape (southern Tian Shan, China). *J. Geophys. Res. Solid Earth* 112 (B3). doi:10.1029/2006jb004362

Hudec, M. R., and Jackson, M. P. (2007). Terra infirma: understanding salt tectonics. *Earth-Science Rev.* 82 (1–2), 1–28. doi:10.1016/j.earscirev.2007.01.001

Izquierdo-Llavall, E., Roca, E., Xie, H. w., Pla, O., Muñoz, J. A., Rowan, M. G., et al. (2018). Influence of overlapping décollements, syntectonic sedimentation, and structural inheritance in the evolution of a contractional system: the central Kuqa foldfold-and-thrust belt (tian Shan mountains, NW China). *Tectonics* 37 (8), 2608–2632. doi:10.1029/2017tc004928

Jiao, L., Klinger, Y., and Scholtes, L. (2021). Fault segmentation pattern controlled by thickness of brittle crust. *Geophys. Res. Lett.* 48 (19), e2021GL093390. doi:10.1029/2021gl093390

Konstantinovskaya, E., and Malavieille, J. (2011). Thrust wedges with décollement levels and syntectonic erosion: a view from analog models. *Tectonophysics* 502 (3–4), 336–350. doi:10.1016/j.tecto.2011.01.020

Lacombe, O., Ford, M., Masini, E., Vergés, J., Pik, R., Ternois, S., et al. (2022). Evolution of a low convergence collisional orogen: a review of Pyrenean orogenesis. *BSGF - Earth Sci. Bull.* 193, 19. doi:10.1051/bsgf/2022018

Le Garzic, E., Vergés, J., Sapin, F., Saura, E., Meresse, F., and Ringenbach, J. C. (2019). Evolution of the NW Zagros Fold-and-Thrust Belt in Kurdistan Region of Iraq from balanced and restored crustal-scale sections and forward modeling. *J. Struct. Geol.* 124, 51–69. doi:10.1016/j.jsg.2019.04.006

Li, C., Yin, H., Wu, Z., Zhou, P., Wang, W., Ren, R., et al. (2021). Effects of salt thickness on the structural deformation of foreland fold-and-thrust belt in the Kuqa depression, Tarim basin: insights from discrete element models. *Front. Earth Sci.* 9. doi:10.3389/feart.2021.655173

Li, J., Webb, A. A. G., Mao, X., Eckhoff, I., Colón, C., Zhang, K., et al. (2014). Active surface salt structures of the western Kuqa fold-thrust belt, northwestern China. *Geosphere* 10 (6), 1219–1234. doi:10.1130/ges01021.1

Li, S. q., Wang, X., and Suppe, J. (2012). Compressional salt tectonics and synkinematic strata of the western Kuqa foreland basin, southern Tian Shan, China. *Basin Res.* 24 (4), 475–497. doi:10.1111/j.1365-2117.2011.00531.x

Li, W., Liu, S., Wang, Y., Qian, T., and Gao, T. (2017). Duplex thrusting in the South Dabashan arcuate belt, central China. *J. Struct. Geol.* 103, 120–136. doi:10.1016/j.jsg.2017.09.007

Liu, C.-y., Huang, L., Zhao, H.-g., Wang, J.-q., Zhang, L., Deng, Y., et al. (2019). Small-scale petroliferous basins in China: characteristics and hydrocarbon occurrence. *AAPG Bull.* 103 (9), 2139–2175. doi:10.1306/0130191608217014

Long, Y., Chen, H. l., Cheng, X. G., Deng, H. D., and Lin, X. B. (2021). Influence of paleo-uplift on structural deformation of salt-bearing fold-and-thrust belt: insights from physical modeling. *J. Struct. Geol.* 153, 104445. doi:10.1016/j.jsg.2021.104445

Lu, R., Xu, X., He, D., Liu, B., Tan, X., and Wang, X. (2016). Coseismic and blind fault of the 2015 Pishan*w*6.5 earthquake: implications for the sedimentary-tectonic framework of the western Kunlun Mountains, northern Tibetan Plateau: western kunlun mountains. *Tectonics* 35 (4), 956–964. doi:10.1002/2015tc004053

Marshak, S., and Wilkerson, M. S. (1992). Effect of overburden thickness on thrust belt geometry and development. *Tectonics* 11 (3), 560–566. doi:10.1029/92tc00175

Maxwell, S. A. (2009). *Deformation styles of allochthonous salt sheets during differential loading conditions: insights from discrete element models*. Rice University.

McQuarrie, N. (2004). Crustal scale geometry of the Zagros fold–thrust belt, Iran. *J. Struct. Geol.* 26 (3), 519–535. doi:10.1016/j.jsg.2003.08.009

Mitra, S. (1986). Duplex structures and imbricate thrust systems: geometry, structural position, and hydrocarbon potential. *AAPG Bull.* 70 (9), 1087–1112. doi:10.1306/94886a7e-1704-11d7-8645000102c1865d

Morgan, J. K. (2015). Effects of cohesion on the structural and mechanical evolution of fold and thrust belts and contractional wedges: discrete element simulations. *J. Geophys. Res. Solid Earth* 120 (5), 3870–3896. doi:10.1002/2014jb011455

Morgan, J. K., and Bangs, N. L. (2017). Recognizing seamount-forearc collisions at accretionary margins: insights from discrete numerical simulations. *Geology* 45 (7), 635–638. doi:10.1130/g38923.1

Muñoz, J. A., Beamud, E., Fernández, O., Arbués, P., Dinarès-Turell, J., and Poblet, J. (2013). The Ainsa Fold and thrust oblique zone of the central Pyrenees: kinematics of a curved contractional system from paleomagnetic and structural data. *Tectonics* 32 (5), 1142–1175. doi:10.1002/tect.20070

Neng, Y., Xie, H. w., Yin, H. w., Li, Y., and Wang, W. (2018). Effect of basement structure and salt tectonics on deformation styles along strike: an example from the Kuqa fold–thrust belt, West China. *Tectonophysics* 730, 114–131. doi:10.1016/j.tecto.2018.02.006

Pla, O., Roca, E., Xie, H. w., Izquierdo-Llavall, E., Muñoz, J. A., Rowan, M. G., et al. (2019). Influence of syntectonic sedimentation and décollement rheology on the geometry and evolution of orogenic wedges: analog modeling of the Kuqa foldfold-and-thrust belt (NW China). *Tectonics* 38 (8), 2727–2755. doi:10.1029/2018tc005386

Qayyum, M., Spratt, D. A., Dixon, J. M., and Lawrence, R. D. (2015). Displacement transfer from fault-bend to fault-propagation fold geometry: an example from the Himalayan thrust front. *J. Struct. Geol.* 77, 260–276. doi:10.1016/j.jsg.2014.10.010

Qi, J., Li, Y., Xu, Z., Yang, S., and Sun, T. (2023). A structural interpretation model and restoration of the mesozoic proto-basin for the Kuqa depression, Tarim basin. *Acta Geol. Sinica-English Ed.* 97 (1), 207–225. doi:10.1111/1755-6724.14963

Ruh, J. B., Kaus, B. J. P., and Burg, J.-P. (2012). Numerical investigation of deformation mechanics in fold-and-thrust belts: influence of rheology of single and multiple décollements. *Tectonics* 31 (3), n/a. doi:10.1029/2011tc003047

Ryan, L., Magee, C., and Jackson, C. A. L. (2017). The kinematics of normal faults in the Ceduna Subbasin, offshore southern Australia: implications for hydrocarbon trapping in a frontier basin. *AAPG Bull.* 101 (03), 321–341. doi:10.1306/08051615234

Santolaria, P., Harris, L. B., Casas, A. M., and Soto, R. (2022). Influence of décollement-cover thickness variations in fold-and-thrust belts: insights from centrifuge analog modeling. *J. Struct. Geol.* 163, 104704. doi:10.1016/j.jsg.2022.104704

Santolaria, P., Izquierdo-Llavall, E., Soto, R., Román-Berdiel, T., and Casas-Sainz, A. (2024). Origin of oblique structures controlled by pre-tectonic thickness variations in frictional and salt-bearing fold-and-thrust belts: insights from analogue modelling. *J. Struct. Geol.* 179, 105042. doi:10.1016/j.jsg.2023.105042

Sherkati, S., Letouzey, J., and Frizon de Lamotte, D. (2006). Central Zagros fold-thrust belt (Iran): new insights from seismic data, field observation, and sandbox modeling. *Tectonics* 25 (4), n/a. doi:10.1029/2004tc001766

Soto, R., Casas, A., Storti, F., and Faccenna, C. (2002). Role of lateral thickness variations on the development of oblique structures at the Western end of the South Pyrenean Central Unit: tectonophysics. *Tectonophysics* 350 (3), 215–235. doi:10.1016/S0040-1951(02)00116-6

Sun, C., Jia, D., Yin, H., Chen, Z., Li, Z., Shen, L., et al. (2016). Sandbox modeling of evolving thrust wedges with different preexisting topographic relief: implications for the Longmen Shan thrust belt, eastern Tibet. *J. Geophys. Res. Solid Earth* 121 (6), 4591–4614. doi:10.1002/2016jb013013

Sussman, A. J., Butler, R. F., Dinarès-Turell, J., and Vergés, J. (2004). Vertical-axis rotation of a foreland fold and implications for orogenic curvature: an example from the Southern Pyrenees, Spain. *Earth Planet. Sci. Lett.* 218 (3-4), 435–449. doi:10.1016/s0012-821x(03)00644-7

Tang, L. J., Jia, C. Z., Jin, Z. J., Chen, S. P., Pi, X. J., and Xie, H. W. (2004a). Salt tectonic evolution and hydrocarbon accumulation of Kuqa foreland fold belt, Tarim Basin, NW China. *J. Petroleum Sci. Eng.* 41 (1–3), 97–108. doi:10.1016/s0920-4105(03)00146-3

Tang, L. J., Jin, Z. J., Jia, C. Z., Pi, X. J., Chen, S. P., Xie, H. W., et al. (2004b). A large-scale tertiary salt nappe complex in the leading edge of the Kuqa foreland fold-thrust belt, the Tarim basin, northwest China: acta geologica sinica-English edition. *Bull. Geol. Soc. China* 78 (3), 691–698. doi:10.1111/j.1755-6724.2004.tb00184.x

Wang, M., Wang, M., Feng, W., Yan, B., and Jia, D. (2022). Influence of surface processes on strain localization and seismic activity in the longmen Shan fold-and-thrust belt: insights from discrete-element modeling. *Tectonics* 41 (11), e2022TC007515. doi:10.1029/2022tc007515

Wang, W., Xie, H., Yin, H., Jia, D., Xu, Z., Luo, H., et al. (2023). Structural variation between the western and eastern Kuqa foldfold-and-thrust belt, China: insights from seismic interpretation and analog modeling. *Acta Geol. Sinica-English Ed.* 97 (4), 1078–1093. doi:10.1111/1755-6724.15074

Wang, W., Yin, H. w., Jia, D., and Li, C. s. (2017). A sub-salt structural model of the Kelasu structure in the Kuqa foreland basin, northwest China. *Mar. Petroleum Geol.* 88, 115–126. doi:10.1016/j.marpetgeo.2017.08.008

Wang, W., Yin, H. w., Jia, D., Neng, Y., Zhou, P., Chen, W. l., et al. (2020). Along-strike structural variation in a salt-influenced fold and thrust belt: analysis of the Kuqa depression. *Tectonophysics* 786, 228456. doi:10.1016/j.tecto.2020.228456

Wang, X., John, S., Guan, S., Hubert-Ferrari, A., Gonzalez-Mieres, R., and Jia, C. (2011). *Cenozoic structure and tectonic evolution of the Kuqa fold belt*. China: Southern Tianshan.

Wu, Z., Yin, H., Wang, X., Zhao, B., and Jia, D. (2014). Characteristics and deformation mechanism of salt-related structures in the western Kuqa depression, Tarim basin: insights from scaled sandbox modeling. *Tectonophysics* 612-613, 81–96. doi:10.1016/j.tecto.2013.11.040

Yang, K., Qi, J., Xu, L., Yu, Y., Sun, T., Shen, F., et al. (2024). Influence of preexisting structures on salt structures in the Kuqa Depression, Tarim Basin, Western China: insights from seismic data and numerical simulations. *Basin Res.* 36 (1). doi:10.1111/bre.12850

Yin, A. (2006). Cenozoic tectonic evolution of the Himalayan orogen as constrained by along-strike variation of structural geometry, exhumation history, and foreland sedimentation. *Earth-Science Rev.* 76 (1-2), 1–131. doi:10.1016/j.earscirev.2005.05.004

Yu, Y. x., Tang, L. j., Yang, W. j., Jin, W. z., Peng, G. x., and Lei, G. l. (2008). Thick-skinned contractional salt structures in the Kuqa depression, the northern Tarim basin: constraints from physical experiments. *Acta Geol. Sinica-English Ed.* 82 (2), 327–333. doi:10.1111/j.1755-6724.2008.tb00582.x

Zhang, J., Morgan, J. K., Gray, G. G., Harkins, N. W., Sanz, P. F., and Chikichev, I. (2013). Comparative FEM and DEM modeling of basement-involved thrust structures, with application to Sheep Mountain, Greybull area, Wyoming. *Tectonophysics* 608, 408–417. doi:10.1016/j.tecto.2013.09.006

Zhang, Y., Yang, S., Chen, H., Dilek, Y., Cheng, X., Lin, X., et al. (2019). The effect of overburden thickness on deformation mechanisms in the Keping fold-thrust belt, southwestern Chinese Tian Shan Mountains: insights from analogue modeling. *Tectonophysics* 753, 79–92. doi:10.1016/j.tecto.2019.01.005

Zhou, C., and Zhou, J. (2022). Relationship between lateral/basal shear stress ratio and structural vergence of thrust wedges: results from analogue modeling and implications for the origin of eastern sichuan–xuefeng fold-thrust belt in south China. *Tectonics* 41 (3). doi:10.1029/2021tc007035